The structure of vanadium oxide species on γ-alumina; an *in situ* X-ray absorption study during catalytic oxidation *

M. Ruitenbeek [a,**], A.J. van Dillen [a], F.M.F. de Groot [a], I.E. Wachs [b], J.W. Geus [a] and D.C. Koningsberger [a]

[a] *Department of Inorganic Chemistry and Catalysis, Debye Institute, Utrecht University, PO Box 80083, 3508 TB Utrecht, The Netherlands*
[b] *Zettlemoyer Center for Surface Studies, Department of Chemical Engineering, Lehigh University, 7 Asa Drive, Bethlehem, PA 18015, USA*

The mechanism of catalytic oxidation reactions was studied using *in situ* X-ray absorption spectroscopy (XAFS) over a 17.5 wt% V_2O_5/Al_2O_3 catalyst, i.e., at reaction temperatures and in the presence of reactants. It was found that X-ray absorption near-edge structure (XANES) is a powerful tool to study changes in the local environment and the oxidation state of the vanadium centres during catalytic oxidation. At 623 K, the catalyst follows the associative mechanism in CO oxidation. XAFS revealed that the Mars–van Krevelen mechanism is operative at 723 K for CO oxidation. The extended X-ray absorption fine structure (EXAFS) results showed that the structure of the supported V_2O_5 phase consists of monomeric tetrahedral $(Al–O)_3–V{=}O$ units after dehydration in air at 623 K. However, the residuals of the EXAFS analysis indicate that an extra contribution has to be accounted for. This contribution probably consists of polymeric vanadate species. The structure remains unchanged during steady-state CO oxidation at 623 and 723 K. Furthermore, when oxygen was removed from the feed at 623 K, no changes in the spectra occurred. However, when oxygen is removed from the feed at 723 K, reduction of the vanadium species was observed, i.e., the vanadyl oxygen atom is removed. The V^{3+} ion subsequently migrates into the γ-Al_2O_3 lattice, where it is positioned at an Al^{3+} octahedral position. This migration process appears to be reversible; so the $(Al–O)_3–V{=}O$ units are thus restored by re-oxidation.

Keywords: V_2O_5, supported catalyst, γ-Al_2O_3, monolayer, CO oxidation, X-ray absorption spectroscopy, XANES, EXAFS, principal component analysis, temperature-programmed reduction

1. Introduction

The molecular structures of surface vanadia species have been extensively investigated in the past few years with many different spectroscopic methods: Raman [1–4], IR [1,5,6], XANES/EXAFS [1,7–11,57], solid state ^{51}V NMR [12–15], UV-VIS DRS [1,16–18], chemi-luminescence [19,20], and ESR [18,21,22]. The local structure of V_2O_5 supported on silica and γ-alumina has been most intensively studied. In general, ESR and UV/VIS results are consistent with each other, although ESR results are restricted to paramagnetic V^{4+} containing species. On silica, vanadium atoms are generally stabilised in an oxygen tetrahedron in the dehydrated state. Hydrated silica-supported V_2O_5 mostly exists in an octahedral configuration.

On alumina, both ESR and UV/VIS studies demonstrated that vanadium is five- or six-fold co-ordinated by oxygen. However, Raman studies revealed the formation of different types of vanadium oxide species: polymeric arrays of octahedral VO_6 units as the main phase and tetrahedral VO_4 species as a minor constituent on both, silica and alumina [4].

Unfortunately, the dynamic nature of the surface vanadia species has resulted in confusion in the published literature, since many studies have compared measurements taken under different experimental conditions (ambient vs. *in situ*, hydrated vs. dehydrated) [23,24].

Most of the early studies were performed with samples exposed to atmospheric air. There is considerable evidence that under these conditions monolayer species react with atmospheric moisture and, therefore, hydrated structures are assumed [25,26]. Under hydrous conditions, the VO_x species may be properly formulated as structure (B) or (C) in figure 1. On heating in a dry atmosphere, dehydration may take place to structure (A) and/or to an octahedral polyvanadate species, such as structure (D) [27,28], or to a simple vanadyl species [29]. *In situ* Raman experiments generally show a shift of the Raman bands due to dehydration of monolayer species [23,25].

In a recent review, Wachs et al. stated that dehydrated surface vanadia species on Al_2O_3, TiO_2, ZrO_2, Nb_2O_5, and CeO_2 all possess identical molecular structures [23]. On these oxidic supports mainly isolated VO_4 units would be present. Their ^{18}O isotopic labelling experiments demonstrated that these surface vanadia species possess only one terminal V=O bond [30,31]. Therefore, Wachs and co-workers tentatively assume that the molecular structures of these surface vanadia species consist of a terminal V=O bond and three bridging V–O-support bonds for the isolated species by (structure (E) in figure 1). Furthermore, a small amount of polymerised species is present, which consist of a terminal V=O bond with one bridging V–O-support bond and two bridging V–O–V bonds [23]. The latter resembles structure (D) in figure 1.

* Netherlands Institute for Research in Catalysis (NIOK) publications #UU 99-1-08 and 99-2-03.

** To whom correspondence should be addressed. Present address: DSM Research, PO Box 18, 6160 MD Geleen, The Netherlands.

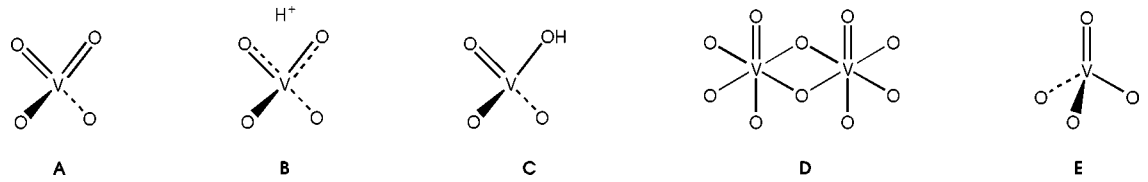

Figure 1. Possible structures for VO_x species in the monolayer phase.

Supported vanadium oxide catalysts are widely used for catalytic partial oxidation of hydrocarbons [32,33], photo-oxidation [34,35], selective catalytic reduction of NO_x [36] and the oxidation of benzene to phenol with N_2O [37]. The reaction path of these kinds of reactions is often related to the Mars–van Krevelen mechanism (*vide infra*). One can distinguish several different reaction steps in catalytic oxidation reactions. Besides redox reactions, such as reduction and oxidation of the catalyst surface, acid–base reactions between reactants and products, on the one, and the catalyst, on the other hand, can take place. Combinations of such steps lead to different overall-reaction mechanisms. Golodets has divided these possible mechanisms in four different groups, which are schematically represented in figure 2 [38].

At elevated temperatures ($T > 773$ K), reactions with the participation of free radicals in the gas phase take place. At moderate temperatures ($573 < T < 773$ K), mostly the Mars–van Krevelen mechanism proceeds. At low temperatures ($T < 373$ K), reactions generally occur through a peroxidic mechanism in which adsorbed radicals are involved.

The most studied mechanism is the above type IIa mechanism. Mars and van Krevelen were the first to have demonstrated this two-step consecutive mechanism for the oxidation of naphthalene [39]. This so-called Mars–van Krevelen or redox mechanism is operative at moderate temperatures. It is schematically represented in figure 3.

The mechanism can best be defined as *a mechanism in which one of the products leaves the surface, containing one of the constituents of the lattice*. With this definition, not only oxidation, reduction, de-oxygenation and oxidative dehydrogenation can be described, but also, e.g., chlorination, dechlorination and hydrodesulphurisation. The latter reactions frequently obey the Mars–van Krevelen kinetics without consumption of oxygen from the lattice of the catalyst.

First, the reactant to be oxidised is adsorbed on the surface of the catalyst resulting in the formation of an adsorbed complex. Subsequently a reaction takes place between the adsorbate and oxygen from the lattice of the catalyst, resulting in the formation of a (partially) oxidised product, which after desorption leaves an oxygen vacancy at the surface. Re-oxidation of this vacancy takes place via gas phase oxygen, as represented in figure 3. If diffusion of lattice oxygen is sufficiently fast, the O^{2-} surface species will migrate into the lattice. This process can continuously take place as long as reactants are present to reduce the catalyst and oxygen to re-oxidise the surface. The presence of metal ions of which the lower oxidation state is relatively stable is a prerequisite for the development of this mechanism.

In general, the Mars–van Krevelen mechanism is assumed to be operative for selective oxidation reactions. At the same time, the complex surface re-oxidation mechanism (type IIb) can play an important role. In this mechanism, formation of the final oxidation products occurs simultaneously with re-oxidation of the surface in a single concerted step. This mechanism is responsible for the formation of total oxidation products [38].

The surface of a metal oxide catalyst is likely to contain an amount of metal ions of a lower oxidation state. Up to a certain concentration, these metal sites can be considered as defects in the metal oxide matrix. However, when the oxygen vacancy concentration becomes too high, a new

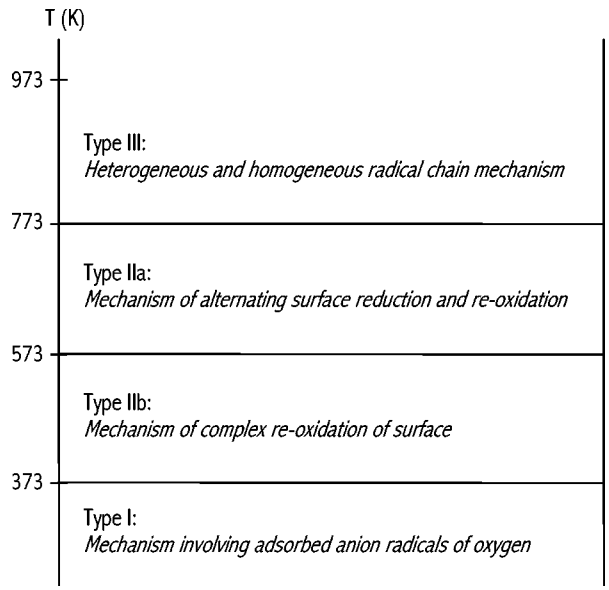

Figure 2. Different types of mechanisms of oxidation reactions as a function of temperature, according to Golodets [38].

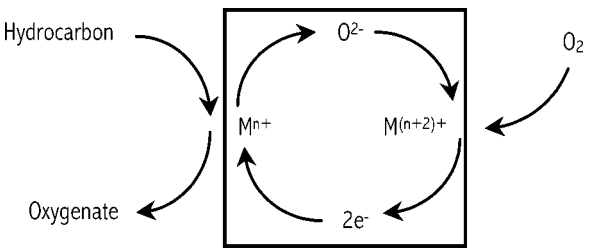

Figure 3. Schematic representation of the redox or Mars–van Krevelen oxidation mechanism (type IIa in figure 2).

$$M^{n+} + O_2 \rightarrow M^{m+}\text{–}O_2^- \quad \text{(a)}$$

$$M^{n+} + M^{m+}\text{–}O_2^- \rightarrow 2[M^{m+}\text{–}O^-] \quad \text{(b)}$$

$$M^{m+}\text{–}O^- + R \rightarrow RO + M^{n+} \quad \text{(c)}$$

Figure 4. Detailed scheme of the associative mechanism (type IIb in figure 2).

solid phase can form. Formation of a new solid phase generally calls for a nucleation step, which usually proceeds too slowly to give rise to a marked catalytic activity. If the redox mechanism is to be operative, it is undesirable that (part of) the catalyst becomes crystalline. Catalysts exhibiting the Mars–van Krevelen mechanism therefore should be able to contain a certain amount of lattice defects without recrystallising into a metal suboxide.

Van Dillen has shown that a marked concentration of oxygen vacancies is attained only at elevated temperatures [40]. Lowering of this temperature by modification of the catalyst results in a more favourable catalytic performance. This suggests that the catalytic activity can be predicted from the thermodynamic stability of non-stoichiometric oxides. In general, however, transition metal oxides also exhibit a significant activity at temperatures where non-stoichiometry is thermodynamically less favoured. Under these conditions, the so-called associative mechanism (type IIb) is believed to be operating.

As indicated in figure 4, after adsorption of molecular oxygen an electron is transferred from a neighbouring metal ion to the oxygen molecule, resulting in the formation of an adsorbed superoxide anion, O_2^-. Dissociation of this ion into two O^- species is followed by a rapid oxidation of the reactant. Because this oxygen sequence is not in equilibrium, the rate of reaction with the reactant is sufficiently high to prevent formation of O^{2-} and subsequent exchange with the lattice.

X-ray absorption near-edge structure (XANES) has long been known to be rich in chemical and structural information [41]. For instance, it provides information about the oxidation state of vanadium. The main indication of the oxidation state of the vanadium atoms is the position of the K-edge in the spectrum. A higher valence state implies a lower energy of the core electron levels and, consequently, the presence of the K-edge at a higher energy [42–45].

Also the pre-edge of the spectrum, which reflects transitions from the K-shell to empty bound d-levels, provides information about the oxidation state of vanadium. Oxidation generally brings about an increase in the intensity of the pre-edge peak, though an effect of the surroundings of the vanadium ions has to be taken into consideration too [42–44]. Therefore, X-ray absorption spectroscopy has proven to be very suitable to study the oxidation state and the local atomic geometry of the vanadium sites in our catalysts *in situ*, i.e., at reaction temperatures and in the presence of reactants.

In the past, we have studied the mechanism of n-butane oxidation to maleic anhydride over a titania-supported V–P–O catalyst with *in situ* X-ray absorption spectroscopy

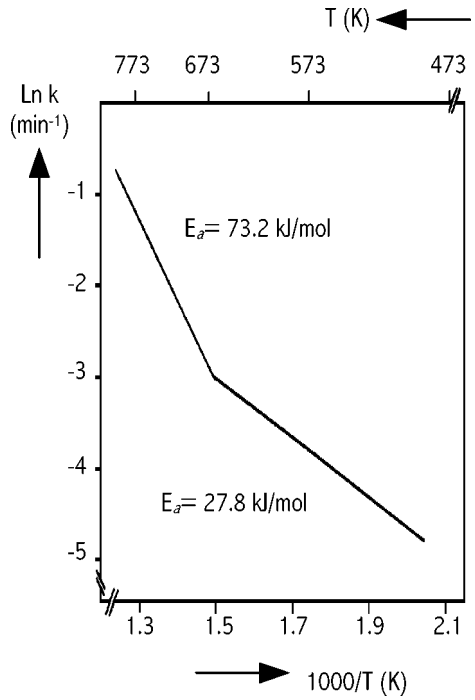

Figure 5. Catalytic data of 7.94 wt% V_2O_5/Al_2O_3. Data and figures were taken from reference [47].

(XANES) in the presence of *n*-butane and air at 553 K [46]. It was found that the average oxidation state of the vanadium atoms in the catalyst did not change any more after several reduction/re-oxidation cycles [46]. This strongly indicates that the generally assumed Mars–van Krevelen mechanism is not operating with this catalyst system. However, it was under debate whether XANES is a proper tool to study the mechanism of oxidation reactions in detail. We realise that the investigation of oxidation reaction mechanisms should not be performed without additional $^{18}O/^{16}O$ scrambling experiments and kinetic measurements. Therefore, we have used a V_2O_5-on-alumina catalyst to proof the principle of mechanistic research with XAFS spectroscopy. This catalyst system is well known for activity in H_2 and CO oxidation [47] and n-butane oxidation [48] and has been extensively characterised [48]. The catalyst was proven to consist of a highly dispersed supported vanadium oxide phase [48]. This is an important condition for the use of X-ray absorption spectroscopy in catalysis, since this technique monitors all vanadium atoms including possible not-active bulk structures.

Van den Berg has determined the activity of a 7.94 wt% V_2O_5-on-alumina catalyst for oxidation of carbon monoxide [47]. Data were corrected for the activity of the support, because it was found that the activity of the support was not negligible. The results of Van den Berg are represented in figure 5.

The data show that the Arrhenius plot for the oxidation of CO consist of two straight lines [47]. Below about 657 K, the activation energy was found to be 28 kJ/mol, whereas at higher temperatures a value of 73 kJ/mol was calculated. The latter activation energy agrees well with

the value measured with defect-rich V_2O_5 [47]. Furthermore, Van den Berg showed that the two different sets of activation energies and pre-exponential factors were not accompanied by different reaction orders [47], which implies that indeed two different mechanisms are operative.

The present chapter deals with the *in situ* characterisation of a 17.5 wt% V_2O_5-on-Al_2O_3 catalyst. The sample was studied with *in situ* X-ray absorption spectroscopy after different pre-treatment procedures and during catalytic oxidation of CO and n-C_4H_{10}. Furthermore, the structure of the catalyst was studied after removal of oxygen from the feed. When the associative mechanism is viable, removal of oxygen should have no or only little impact on the spectra. However, when the Mars–van Krevelen mechanism is operating, these oxygen-free conditions should result in reduction of the sample. Consequently, structural changes of the VO_x phase are expected and these should be observable in both the XANES and EXAFS part of the XAFS spectra of the catalyst.

Additional TPR/TPO experiments and principal component analysis (PCA) were performed to support the X-ray absorption spectroscopy results. It will be shown that the structure of the supported VO_x species strongly depends on the employed conditions (dehydration, oxidation and reduction). The structural changes upon reduction of the specimen will be dealt with, and a model of the reduced VO_x structure will be presented. As far as we know, no characterisation of the reduced vanadium oxide phase has been reported in the literature [24].

2. Experimental

2.1. Sample preparation

17.5 wt% V_2O_5 on alumina (Harshaw, $\sim$180 m^2/g) was prepared by incipient-wetness impregnation. A vanadium(III) isopropoxide (Alfa, 95–99% purity) in methanol (Fisher, 99.9% purity) solution was used to impregnate the oxide support in a nitrogen environment. The sample was first dried in N_2 at room temperature for 2 h to remove excess methanol and further dried at 393 K for 16 h under flowing N_2. The samples were finally kept at 773 K for 1 h under flowing N_2 and an additional 15 h under flowing dry air to form surface vanadium oxide species.

2.2. XANES/EXAFS experiments

V K-edge absorption spectra were taken at station 8.1 of the SRS in Daresbury (UK), using a Si(111) double crystal monochromator. The measurements were generally performed in transmission mode using ion chambers filled with Ar to have a μx of 20 and 80% in the first and second ionisation chamber, respectively. The monochromator was detuned to 50% of maximum intensity at the V K-edge (5465 eV) to minimise the presence of higher harmonics.

To minimise high and low frequency noise the counting time per data point was 1000 ms and at least four scans were averaged. A vanadium metal foil of 5 μm was used for calibration of the edge position. Absorption spectra were calibrated at the position of the main-edge jump of vanadium at 5465 eV according to Wong et al. [42,44].

The sample was pressed into a self-supporting wafer and mounted in an *in situ* EXAFS cell [49,50], equipped with beryllium windows. The thickness of the wafer was chosen to give an absorption (μx) of 2.5 at the absorption edge for optimal signal-to-noise ratio. To prevent thickness effects for the highly loaded samples μx was set to yield of a step of 1.0 in absorption in the edge region. Typically, about 20 mg of catalyst was used, accompanied with 40 mg of BN in order to have a manageable amount.

Samples have been studied after several treatments, which are specified in table 1. Prior to these treatments, the sample was prepared and treated as described above. After treatment 1, the sample will be denoted as the fresh

Table 1
Conditions after and during which the X-ray absorption data were collected. All flows were set to about 100 ml/min.

Treatment	Pre-treatment	Measuring conditions
1	15 min He flush at RT	He, 77 K
2	(a) 15 min He flush at RT (b) RT to 723 K (300 K/h) in He (c) Cooldown to RT in He	He, 77 K
3	(a) 15 min He flush at RT (b) RT to 723 K (300 K/h) in air (c) Cooldown to 623 K in air	Air, 623 K
4	(a) Treatment 3 (b) RT to 623 K (300 K/h) in He (c) 30^+ min 1% CO, 5% O_2 in He at 623 K	CO, O_2, He, 623 K
5	(a) Treatment 4 (b) 30^+ min 1% CO in He at 623 K	CO, He, 623 K
6	(a) Treatment 5 (b) 60^+ min 1% CO, 5% O_2 in He at 723 K	CO, O_2, He, 723 K
7	(a) Treatment 6 (b) 30^+ min 1% CO in He at 723 K	CO, He, 723 K

catalyst. Treatments 2 and 3 were dehydration experiments in helium and in air, respectively. The mechanistic studies were started with the dehydration procedure in air (treatment 3). The mechanism of the CO oxidation reaction was studied at two different temperatures, i.e., at 623 and 723 K. The first temperature is well below the temperature corresponding with the kink in the Arrhenius curve (670 K) as observed by Van den Berg and 723 K is above this temperature [47].

Data reduction and data analysis were performed with the XDAP code developed by Vaarkamp et al. [51]. Standard procedures were used to extract the EXAFS data from the measured absorption spectra. The pre-edge was subtracted using a modified Victoreen curve [52] and the background was subtracted using cubic spline routines [53,54]. Normalisation was performed by dividing the data by the height of the absorption edge at 50 eV.

Averaging 3–4 scans of the individual background-subtracted and normalised data attained the final EXAFS function.

Phase shifts and backscattering amplitudes from reference compounds were used to calculate the EXAFS contributions: Na_3VO_4 for the V–O contribution and Ti-foil for the V–V contribution. The co-ordination in vanadium metal is bcc, which implies that there is considerable overlap between the first two co-ordination shells. Therefore, the metal is not suitable for use as a reference compound for the V–V scatterer pair. We have used Ti-foil as a replacement. Titanium is adjacent in the periodical table, and it is assumed that the backscattering amplitude and the phase shift will not differ to a great extent from those of vanadium.

The fit parameters were determined by multiple shell fitting in R-space [55,56]. Backscatterers were identified by applying the difference file technique using phase-corrected Fourier transformations [54,55,57]. The final fit parameters were obtained after a full optimisation of all parameters in both k^1 and k^3 weighting in the Fourier transformations. Variances were calculated according to the methods described by Mojet [56]. The inaccuracies in the fit parameters were estimated to be 20% in co-ordination number (N), 1% in distance (R), 5% in Debye–Waller factor ($\Delta\sigma^2$), and 10% in inner potential correction (ΔE_0).

2.3. Principal component analysis

Principal component analysis (PCA) is a numerical technique that can indicate the number of spectral components that contribute to a series of spectra consisting of different components. The use of PCA is especially valuable in the analysis of EXAFS data, since the distorted nature of oxides makes analysis of the EXAFS data difficult when using traditional curve-fitting methods. Furthermore, it has been applied with XPS data, where the lack of proper reference spectra makes curve-fitting difficult [58–60]. A nice introduction to PCA is outlined by Hercules et al. [58,61]. The requirements for PCA are: (i) the measured spectra are linear sums of the individual components; (ii) the components vary independently; (iii) the data matrix contains more spectra than components [58].

PCA was carried out on $\chi(k)$ spectra using a procedure outlined by Malinowski [62]. First, a data matrix, [D], was constructed from the $\chi(k)$ spectra such that the columns correspond to the individual $\chi(k)$ spectra and the rows to the $\chi(k)$ spectral elements (the data points). The next step usually is to obtain the correlation or covariance values, r_0, by multiplying [D] with its transpose. In general, it is not mandatory for PCA that the spectral elements of $\chi(k)$ occur at identical abscissa intervals [61]. Subsequently, a symmetric square matrix, [Z], is constructed. The [Z] matrix is then decomposed into eigenvectors using an iterative procedure, according to Malinowski [62]. The eigenvectors or abstracted principal components, which represent the signal data in the matrix, can be separated from those which account for random noise. The indicator function (IND) and the F-test are usually chosen as criteria for selecting the number of abstract principal components [61]. IND is an empirical function proposed by Malinowski, which should reach a minimum when the correct number of abstract principal components are considered [62]. The F-test requires evaluation of the F statistics to test two variances [63,64]. The probability that F-values higher than the evaluated F statistic exist is given by α. The null hypothesis is that a given factor is a member of the pool of factors, which are considered as noise. Hence, if α is $\leqslant$ P%, then the associated eigenvector is accepted as an abstract principal component. Generally, the P% test level is 10% [61].

2.4. TPR/TPO experiments

Reduction and re-oxidation of the sample was studied using temperature-programmed reduction and temperature-programmed oxidation. TPR/TPO experiments were carried out with a TPD/R/O 1100 apparatus (Thermoquest/CE instruments). 91.6 mg of the sample (as synthesised) was placed in a quartz tubular reactor and dehydrated by heating at 623 K in air. Subsequently, TPR was performed with a mixture of 5% H_2 in argon (20 ml/min, heating rate 10 K/min). After the first TPR experiment, the sample was cooled down to room temperature and TPO was performed with a mixture of 5% O_2 in He (20 ml/min, heating rate 10 K/min). Subsequently, a second TPR experiment was performed (conditions equal to the first TPR).

3. Results

We will present the results of this investigation in separate sections. These sections are distinguished by the four different types of experiments that we have performed, i.e., dehydration, CO oxidation at 623 K, and CO oxidation at 723 K.

3.1. Dehydration experiments

Figure 6 represents the V K-edge spectra of the fresh 17.5 wt% V_2O_5/Al_2O_3 sample and after the two different thermal pre-treatment procedures, i.e., in He and in air.

The spectrum of the fresh catalyst shows the typical vanadium K-edge spectrum, i.e., a pre-edge peak (5470 eV) peaks at the absorption edge (5480 eV) and peaks at energies more than 10 eV higher than the edge position. It is obvious that the two pre-treatment procedures result in different spectra. The changes of the edge positions as well as the relative intensity of the pre-edge are represented in table 2. Besides the differences in position and intensity of the pre-edge, also the peaks around and beyond the absorption edge show clear differences. Pre-treatment in helium resulted in a shift of the pre-edge to lower energy and a decrease of the pre-edge intensity. During the pre-treatment in air, however, the pre-edge slightly shifted to higher energy and the relative intensity increased.

Figure 7 represents the raw EXAFS functions after or during the different treatments. It is obvious that differences between the three samples are also visible in the EXAFS data. From the spectra in figures 6 and 7, it can be concluded that the dehydration method had a tremendous impact on the final structure of the catalyst sample. Dehydration in helium does not result in the same structure as dehydration in air.

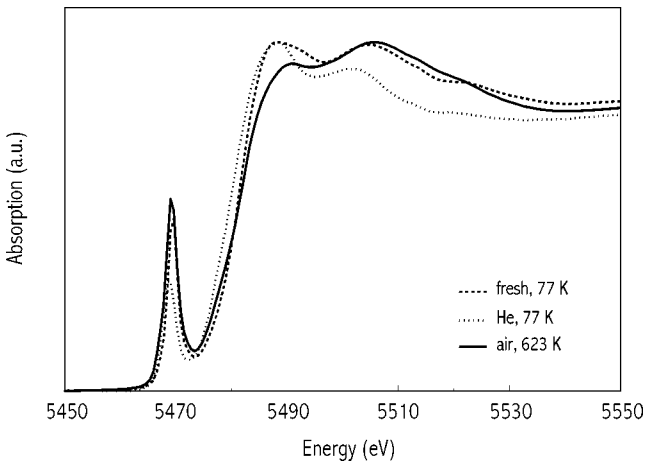

Figure 6. V K-edge spectra of the 17.5 wt% V_2O_5/Al_2O_3 catalyst after different dehydration procedures (for conditions see table 1).

Table 2
Pre-edge positions and relative intensities of the 17.5 wt% V_2O_5/Al_2O_3 sample after/during the different treatments.

Treatment	Conditions	Pre-edge position (eV)	$I_{\text{pre-edge}}/I_{\text{edge}}$
1	Fresh, 77 K	5469.4	0.49
2	He, 77 K	5468.6	0.31
3	Air, 623 K	5469.2	0.55
4	CO, O_2, He, 623 K	5469.2	0.54
5	CO, He, 623 K	5469.2	0.53
6	CO, O_2, He, 723 K	5469.4	0.48
7	CO, He, 723 K	5468.4	0.18

We have determined the structural parameters of the 17.5 wt% V_2O_5/Al_2O_3 sample during the different treatments using a k^2 R-space fit with the difference file technique. This was performed using the XDAP code [51]. The accompanying structural fit parameters are included in table 3.

EXAFS analysis of the hydrated sample (treatment 1) showed one short vanadyl bond at 1.55 Å and a second V–O bond at 1.74 Å. Furthermore, two oxygen neighbours located at 1.90 Å have been found. The k^2 Fourier transform of the raw data and of the best fit of this sample are represented in figure 8. The structure of the sample that was dehydrated in helium (treatment 2) is more complicated. It was not possible to obtain a reliable fit with parameters known from the literature.

After dehydration in air (treatment 3), we observe one short bond of 1.62 Å and three longer bonds of 1.82 Å. This distorted tetrahedron is in agreement with the shape of the XANES for this specimen. The k^2 Fourier transform of the raw data and of the best fit of this sample are represented in figure 9. The sample that had been dehydrated in air has been used for the mechanistic studies.

3.2. CO oxidation at 623 K

In figure 10, the different *in situ* V K-edge spectra of the catalyst during CO oxidation with and without oxygen at 623 K are represented. The spectra show that there are only small differences between the spectra of the dehydrated sample (treatment 3) and the sample during CO oxidation at 623 K (treatments 4 and 5). Moreover, minor changes in the first peaks around the absorption edge are observed. There is almost no difference between the spectra taken during the steady-state experiment or after removal of oxygen from the feed at 623 K.

The sample that was dehydrated in air was used for all further *in situ* experiments. During CO oxidation at 623 K, almost no changes in the spectrum can be observed as represented in figure 11. Bond distances and co-ordination

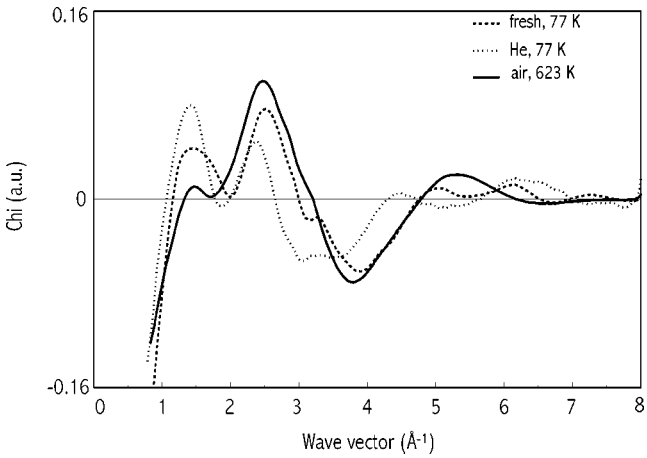

Figure 7. EXAFS spectra of the 17.5 wt% V_2O_5/Al_2O_3 catalyst after different pre-treatment procedures (for conditions see table 1).

Table 3
Structural parameters of the 17.5 wt% V_2O_5/Al_2O_3 sample after different treatments. R = distance, CN = co-ordination number, $\Delta\sigma^2$ = deviation of Debye–Waller factor from Na_3VO_4 reference compound, E_0 = inner-potential correction.

Treatment	Description	Scatterer	R (Å)	CN	$\Delta\sigma^2$	E_0
1	Fresh	O_1	1.55	1.0	−0.01738	−1.21
		O_2	1.74	1.0	−0.01892	4.57
		O_3	1.90	2.0	0.00184	2.01
3	Air, 623 K	O_1	1.62	1.0	−0.00989	0.49
		O_2	1.82	3.0	0.01463	0.84
4	CO, O_2, He, 623 K	O_1	1.62	1.0	−0.00693	2.43
		O_2	1.82	3.1	0.02309	2.16
5	CO, He, 623 K	O_1	1.62	1.0	−0.00651	1.17
		O_2	1.82	3.1	0.02457	2.77
6	CO, O_2, He, 723 K	–[a]	–[a]	–[a]	–[a]	–[a]
7	CO, He, 723 K	O_1	1.97	3.0	−0.00100	−4.85
		O_2	2.10	3.1	0.00138	5.46
		Al_1	2.73	2.9	0.02300	5.71
		Al_2	3.79	1.0	0.00361	1.22

[a] No acceptable fit of data obtained.

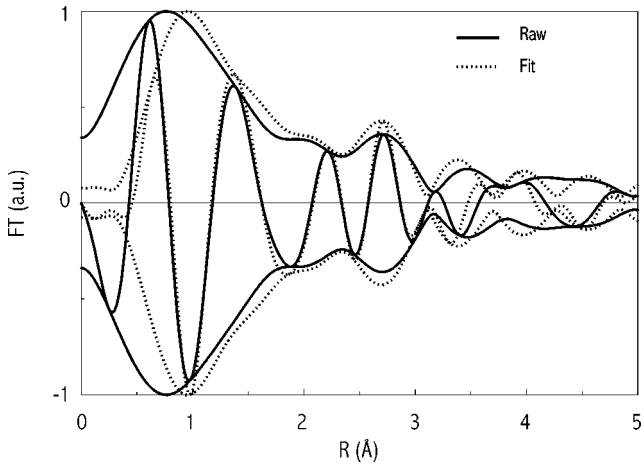

Figure 8. Fourier transforms (k^2, Δk = 2.5–8.0 Å^{-1}, ΔR = 1.0–3.0 Å) of the EXAFS spectrum (solid line) and the best fit (dotted line) of the fresh sample (treatment 1).

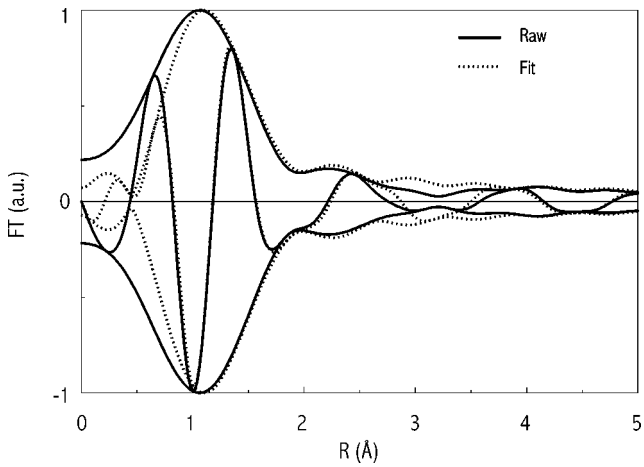

Figure 9. Fourier transforms (k^2, Δk = 2.5–8.0 Å^{-1}, ΔR = 1.0–3.0 Å) of the EXAFS spectrum (solid line) and the best fit (dotted line of the sample that was dehydrated in air (treatment 3).

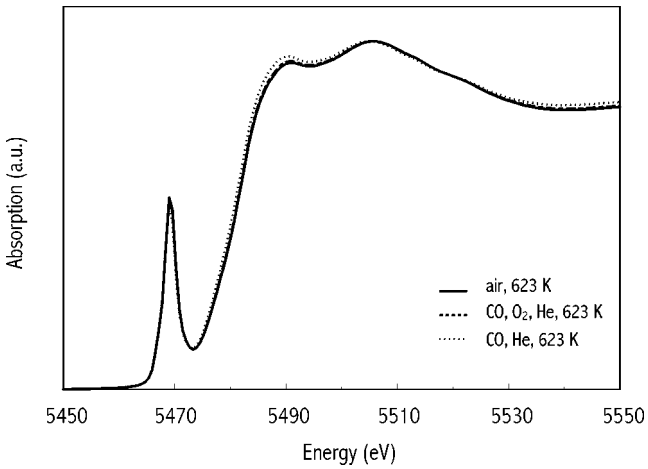

Figure 10. V K-edge spectra of the 17.5 wt% V_2O_5/Al_2O_3 catalyst before and during CO oxidation at 623 K (for conditions see table 1).

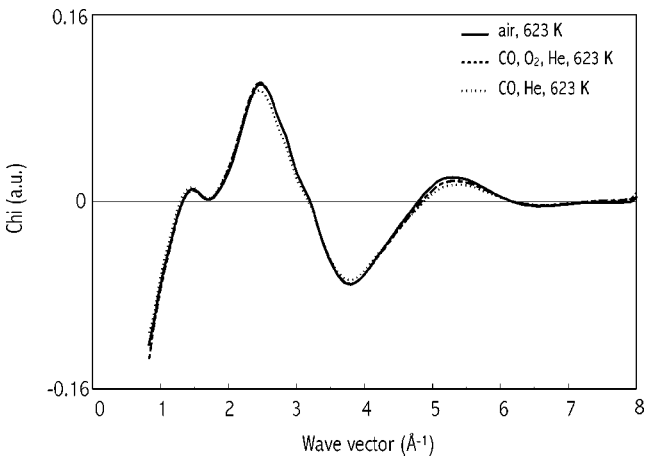

Figure 11. EXAFS spectra of the 17.5 wt% V_2O_5/Al_2O_3 catalyst before and during CO oxidation at 623 K (for conditions see table 1).

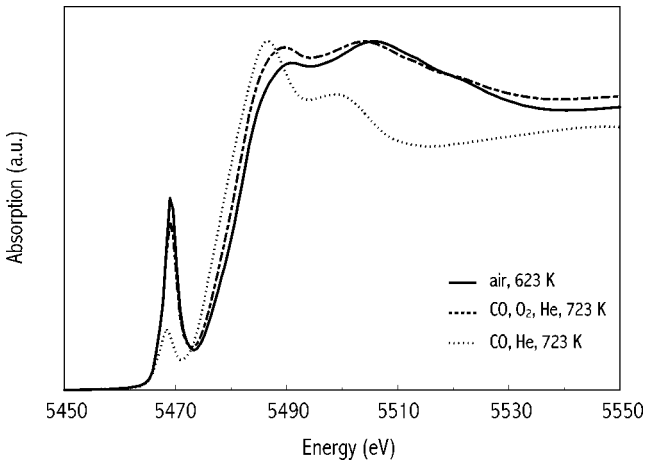

Figure 12. V K-edge spectra of the 17.5 wt% V_2O_5/Al_2O_3 catalyst before and during CO oxidation at 723 K (for conditions see table 1).

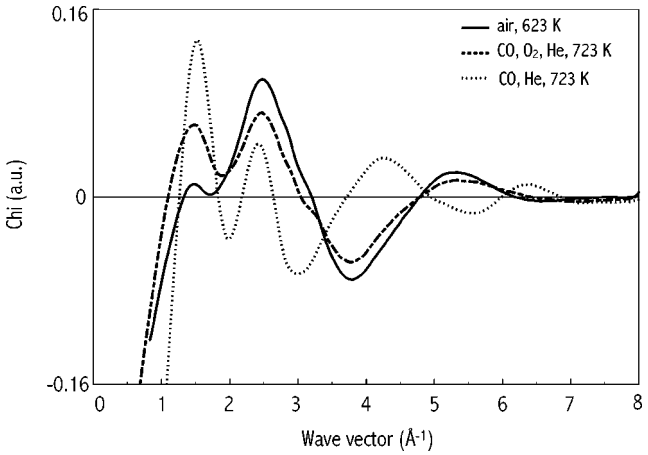

Figure 13. EXAFS spectra of the 17.5 wt% V_2O_5/Al_2O_3 catalyst before and during CO oxidation at 723 K (for conditions see table 1).

numbers remained the same within the experimental error. However, for both V–O contributions, at 1.62 and 1.82 Å, respectively, increased Debye–Waller factors are observed. In the absence of oxygen at 623 K (treatment 5), the catalyst showed a further increase of the Debye–Waller factors, but again, no changes in distance and co-ordination number.

Figures 7, 11, and 13 indicate that the structure of the supported V_2O_5 phase is closely analogous for several differently pre-treated samples. The air-dehydrated sample (treatment 3) and of the samples of the steady-state experiments with CO at 623 and 723 K (treatments 4 and 5) are almost identical. These spectra are assumed to be composed of various distinct V_2O_5 species, i.e., monomeric vanadyl species and polymeric vanadate species [48].

However, it appeared possible to fit the data with one major component, the monomeric vanadyl species. Nevertheless, the residuals indicate that for a proper fit also the polymeric species must be taken into account. To establish the number of species and their relative amount, principal component analysis (PCA) was applied.

Table 4
Principle component analysis of the 17.5 wt% V_2O_5/Al_2O_3 before and during CO oxidation at 623 and 723 K and the first shell fit of the monomeric species. Analysis range = 2.5–8 $Å^{-1}$.

Factor	r_0	IND	F	Q (%)
1	0.72169	1.79×10^{-3}	70.77	0.11
2	0.01794	1.69×10^{-3}	12.52	3.84
3	0.00158	2.87×10^{-3}	2.91	23.01
4	0.00051	4.19×10^{-3}	9.48	19.99
5	0.00003			

In table 4, results of the principle component analysis of a data matrix containing the spectra of treatments 3, 4 and 5, as well as the chi data of the fit of the monomeric species are represented. The spectral window for the analysis was 2.5–8 $Å^{-1}$. The data show a minimum for the indicator function (IND) at the second factor. Furthermore, the Q-test values exceed the 10% margin at the third factor. These results indicate that the spectra of the 17.5 wt% V_2O_5/Al_2O_3 catalyst consists of two components during or after treatments 3, 4, and 5, i.e., the vanadyl monomers and polymeric species, which have not been included in the fit.

3.3. CO oxidation at 723 K

Figure 12 shows the spectra during CO oxidation at 723 K. At 723 K, the spectrum of the first scan was almost equal to the previous spectrum (623 K CO oxidation). However, the two following spectra were already different. This indicates that the sample is changing under the applied conditions. Furthermore, switching off oxygen at 723 K turned out to have a substantial effect on both the pre-edge and the absorption edge itself (figure 11). Both edges shifted to lower energies. Furthermore, the relative intensity of the pre-edge decreased from 0.55 ($I_{\text{pre-edge}}/I_{\text{edge}}$) to 0.18, as indicated in table 2.

In agreement with the XANES spectra, differences were observed between the various scans during the steady-state experiment at 723 K (treatment 6), as indicated in figure 13. This indicates that the structure of the catalyst changed under these conditions. We have performed a CO oxidation experiment in the *in situ* EXAFS cell, connected to an on-line Balzers QMS420 mass spectrometer. Although we realise that the experimental set-up in the EXAFS cell did not meet the ideal microreactor conditions (plug-flow, etc.) [65], the corrected CO conversion was 4% at 623 K and 23% at 723 K. Consequently, the differences in the spectra could be brought about by the different composition of the gas mixtures at different conversion levels.

When oxygen was removed from the feed at 723 K (treatment 7), a more dramatic change of the catalyst structure was observed. This structural change is probably the result of reduction of the vanadium species in the catalyst. Equal results have been obtained in n-butane oxidation at 723 K, although the effects of water have to be taken into account there also [66].

As far as we know, no characterisation of a reduced vanadium oxide phase has been reported in the litera-

ture [24]. Therefore, analysis of the EXAFS data of the reduced phase will provide useful new information. We have fitted the structure of the reduced vanadium oxide phase with three oxygen neighbours at 1.97 Å and three oxygen neighbours at 2.10 Å (distorted octahedral geometry). Furthermore, two vanadium–aluminium contributions were included in the fit, i.e., at 2.73 Å (CN = 3) and at 3.79 Å (CN = 1). The k^2 Fourier transforms of the EXAFS data and of the best fit of this sample are represented in figure 14.

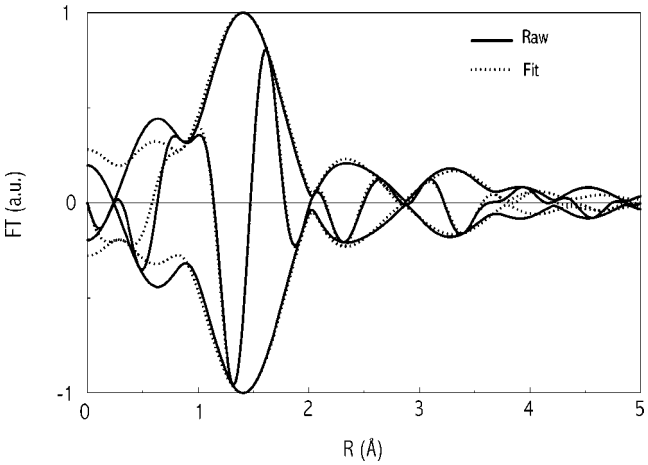

Figure 14. Fourier transforms (k^2, $\Delta k = 2.5$–8.0 Å^{-1}, $\Delta R = 1.0$–3.5 Å) of the EXAFS spectrum (solid line) and the best fit (dotted line) of the sample after reduction in CO at 723 K (treatment 7).

Figure 15 represents the Fourier transforms of the fits of the four contributions in the EXAFS spectrum after reduction in CO at 723 K (solid lines). Furthermore, the Fourier transforms of the raw data minus the other three contributions (dotted lines) are shown for O_1, O_2, Al_1, and Al_2, respectively. The results indicate that the fit of the EXAFS data of the reduced V_2O_5/Al_2O_3 catalyst are excellent. The residuals in the low R range, which can be observed clearly in the fits of Al_1 and Al_2 and to a minor extent in the fit of O_2 are AXAFS (atomic EXAFS) contributions [67]. We will deal with this feature in a forthcoming paper [68].

3.4. Temperature-programmed reduction

Temperature-programmed reduction (TPR) is a technique that provides information about the reducibility of oxidic materials. We have applied TPR to study the struc-

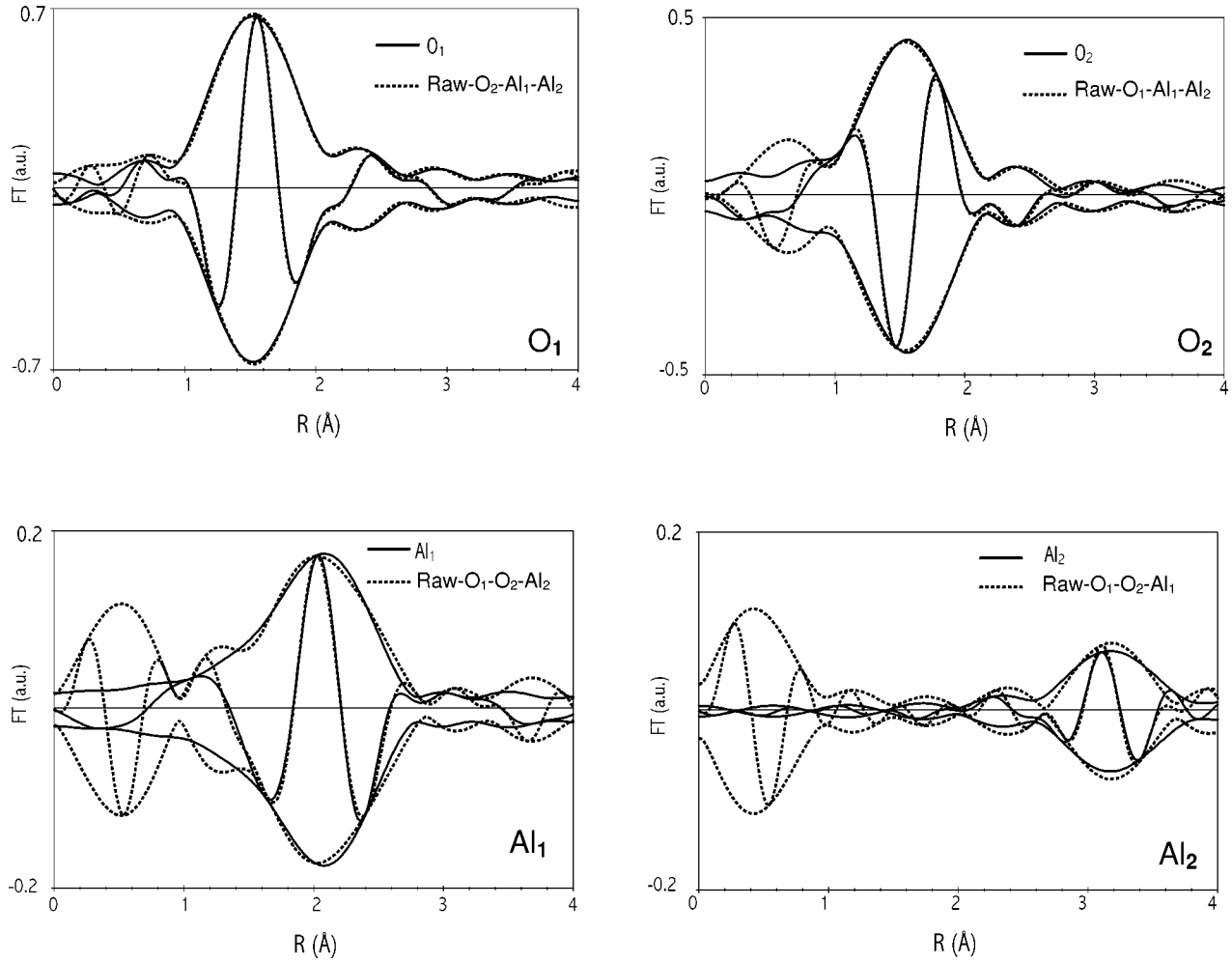

Figure 15. Fourier transforms (k^2, $\Delta k = 2.5$–8.0 Å^{-1}) of the fits of the various shells of the EXAFS spectrum (solid lines) and the raw data minus the fits of the other shells (dotted lines) of the sample after reduction in CO at 723 K (treatment 7).

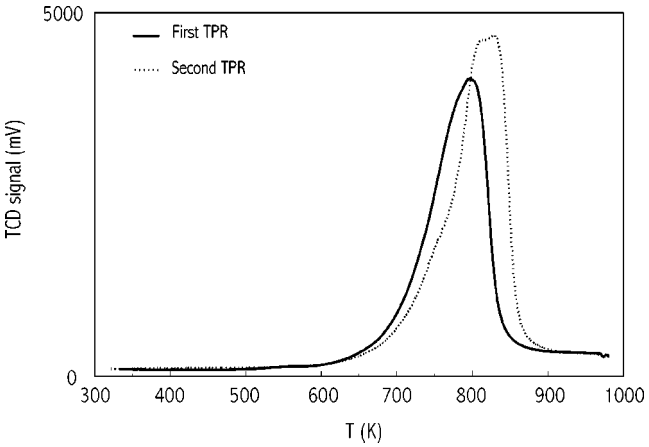

Figure 16. TPR patterns of the 17.5 wt% V_2O_5/Al_2O_3 sample after dehydration (first TPR) and after re-oxidation (second TPR). Between subsequent TPR/TPO/TPR runs, the sample was not exposed to air.

tural changes upon cyclic reduction/re-oxidation experiments. The results could give information about the structure of the reduced vanadium oxide phase as measured with the *in situ* EXAFS experiments.

Figure 16 represents the results of the TPR experiments of the dehydrated catalyst (first TPR). After this experiment, we re-oxidised the specimen and subsequently, performed a second TPR experiment. During the first TPR, one broad asymmetric peak is observed. The onset temperature is about 600 K and the peak maximum is at 800 K. The total integrated intensity of the peak corresponds nicely to a reduction of V^{5+} to V^{3+}.

For the second TPR, the onset temperature is again 600 K, but the T_{max} has shifted to a higher temperature. The differences between the peak areas of the two TPR experiments were about 7%, which is within the experimental error.

4. Discussion

It is well known that the activity and selectivity of supported V_2O_5 catalysts strongly depend on the supports used and the preparation procedures. One of the essential factors in controlling the catalytic performance is the local structure of the vanadium oxide species on the support. The oxygen co-ordination number and the state of aggregation on various supports have been widely studied. For reasons of comparison, we will start the discussion of our results with an overview of what is known in the literature about the structure of supported vanadium(V) oxide. Subsequently we will discuss our results for the different types of experiments (dehydration, CO oxidation at 623 K, CO oxidation at 723 K and C_4H_{10} oxidation at 723 K) and compare the results with literature data. Finally, we will place our results in the framework of the associative mechanism and the Mars–van Krevelen mechanism and propose a model for the structure of the reduced vanadium oxide phase.

4.1. X-ray absorption spectroscopy with (supported) vanadium oxide

Wong et al. have investigated the V K-edge spectra of a broad range of vanadium compounds, including oxides, vanadates, vanadyl compounds and intermetallics in great detail [42,44]. Their study has been of great importance for the interpretation of all later work on V K-edge spectra regarding symmetry, co-ordination geometry, ligand type (N,O) and bond lengths.

Wong et al. distinguished two types of near-edge spectra: (i) octahedrally co-ordinated compounds, such as V_2O_3, etc., which exhibit a weak pre-edge absorption peak, and (ii) tetrahedrally co-ordinated compounds, such as NH_4VO_3, etc., or compounds with a short vanadyl bond in a square pyramid, all of which exhibit a rather strong pre-edge peak [42].

This pre-edge peak is the result of a transition from the 1s state to the total empty manifold of the compound. For a transition metal atom (like vanadium) in octahedral symmetry, the 1s to 3d transition is dipole forbidden, but it is an allowed quadrupole transition [42]. It is weak, but observable. However, in a distorted octahedral environment, mixing of the 3d orbitals with the 4p orbitals takes place [42]. Therefore, the pre-edge peak can be rather strong, as for instance in the spectrum of bulk V_2O_5 [42]. For tetrahedral complexes, the lack of a centre of inversion permits a dipole transition from 1s to the T_2 orbitals, which can possess 4p character in addition to 3d character. This gives rise to the strong pre-edge usually found with these compounds [42].

Various authors have described the application of XAFS to study supported V_2O_5 catalysts. Kozlowski et al. have studied vanadium oxides supported on silica and γ-alumina [10,11]. They found that the main species on alumina are VO_4 dimers with two short (1.67 Å) and two long (1.82 Å) V–O bonds, whereas on silica mainly V_2O_5-like clusters were observed.

Tanaka et al. observed polymeric VO_5 square pyramids on silica and monomeric VO_4 tetrahedrons on alumina under ambient conditions [7]. For the dehydrated samples, VO_4 tetrahedrons were also observed with the alumina-supported catalyst. No octahedral species were found with EXAFS [8]. These species could not be completely excluded, because diffuse reflectance UV-VIS experiments revealed a broad, but small band in the 400–500 nm region [8]. This band was assigned to a charge-transfer band of octahedral VO_6 species [69].

Yoshida et al. have investigated the structural parameters of alumina-supported V_2O_5 in the hydrated and dehydrated state with X-ray absorption spectroscopy [7–9]. However, no clear information about the dehydration procedure has been provided (air or inert). For the dehydrated sample they reported one short V=O bond of 1.63 Å ($\Delta\sigma^2 = -0.0050$) and three longer V–O-support bonds ($R = 1.78$ Å, $\Delta\sigma^2 = 0.0065$). They found that in the hydrated sample, the V=O bond is slightly elongated (1.67 Å), and the Debye–Waller

factor increased to 0.0022 indicating that the oxygen is less tightly bound (structure (B) in figure 1).

Gao et al. have reported XANES data of a 10 wt% vanadium oxide-on-silica-catalyst in the hydrated and dehydrated state, of which the pre-edge position and intensity, as well as the XANES are almost equal to our results [1]. Based on their X-ray absorption spectra and UV-VIS DRS spectra, they concluded that the structure of the dehydrated silica-supported V_2O_5 phase consists of a distorted tetrahedron [1].

4.2. Structure of the supported vanadium oxide phase

Considering our XAFS results, it is obvious that for the 17.5 wt% V_2O_5-on-Al_2O_3 catalyst, a geometry without inversion symmetry is expected in almost all cases. Only the reduced samples, i.e., the samples after dehydration in helium or during CO and n-C_4H_{10} oxidation in the absence of oxygen at 723 K (treatments 2, 7, and 9), show a decreased pre-edge feature that is shifted to lower energies. These results strongly indicate that the preferred geometry of the sample is tetrahedral in the oxidised state, and (distorted) octahedral in the reduced state [70]. In case of complete inversion symmetry, only the quadrupole contributions to the pre-edge peak are observable. For iron-based compounds, this results in an $I_{\text{pre-edge}}/I_{\text{edge}}$ ratio of 0.07 [71]. However, for vanadium compounds, this ratio is not known. Therefore, it is difficult to attribute a specific co-ordination geometry to the reduced VO_x phase. Nonetheless, it is expected that this co-ordination is preferably distorted octahedral.

The results of our *in situ* experiments show that the tetrahedron at the oxidised state is not affected by the conditions during the steady-state oxidation reactions at 623 K. However, under CO oxidation conditions at 723 K (treatment 6) the structure of the supported vanadium oxide phase already changes. When oxygen is removed from the feed at 723 K (treatment 7), the pre-edge peak shifts to lower energy and the intensity decreases. Furthermore, the XANES spectrum changes. These changes indicate that the vanadium geometry changes from distorted tetrahedral to distorted octahedral. These findings are in agreement with the structural parameters obtained from the EXAFS data analysis. We will now discuss the EXAFS results during the different treatments of this investigation.

4.3. Structure before and after dehydration experiments

The XANES spectra of the fresh 17.5 wt% V_2O_5-on-Al_2O_3 catalyst and the spectra that were obtained after the two different dehydration procedures show differences in co-ordination geometry. The fresh, hydrated sample exhibits the characteristic XANES of a VO_5 compound (square pyramidal configuration as in V_2O_5, V_4O_7 or V metal) [42–44]. After dehydration in helium (treatment 2), the XANES spectrum resembles the spectra reported for octahedral (VO_6) compounds [42–44], whereas after dehydration in air (treatment 3), the characteristic spectrum of a tetrahedrally co-ordinated vanadium compound (VO_4) is observed [42–44].

The EXAFS data of our dehydration experiments also display remarkable differences between the spectra of the fresh sample (treatment 1) and the dehydrated samples (treatments 2 and 3). The data for the fresh sample do not match the model proposed by Yoshida and co-workers, i.e., a tetrahedral monomer with elongated vanadium–oxygen bonds. We obtained better results when a model that resembles structure (C) in figure 1 was used. This structure is in agreement with the dehydration model as proposed by Gao et al. for a 10 wt% V_2O_5-on-SiO_2 catalyst [1].

After dehydration in helium, the vanadium species could have been reduced due to removal of the OH groups from the hydrated structure. This is, however, not resulting in the same reduced phase as with the samples reduced by CO. We were not able to obtain a good fit of these data, because defect-rich species have been formed after dehydration in helium. This is probably the result of inhomogeneity of the type of species present after dehydration in helium.

Based on the Raman results of Wachs and co-workers, we expect that a tetrahedral species with one short vanadyl bond and three longer vanadium–oxygen bonds is formed after dehydration in air (treatment 3) [48]. This model is in agreement with our XANES data of this sample. The EXAFS data analysis was successfully performed with a fit consisting of one short vanadyl bond (1.62 Å) and three V–O–Al bonds (1.82 Å). However, the Raman data revealed an additional component in the spectra of the dehydrated sample, i.e., polymerised vanadyl species. Although we obtained a good fit of our raw EXAFS function with only the monomers in our model, we have applied principal component analysis (PCA) to see whether more components are present in the spectrum of the dehydrated sample (treatment 3).

The results of the PCA clearly indicate the presence of a second component in the spectrum of the dehydrated sample. The IND function shows a minimum for the second factor and both, the first and the second factor show a Q (%) of less than 10% which was set as the limit. The eigenvectors indicate that the first factor is the dominant species in the sample. This factor is the monomeric $(Al–O)_3–V{=}O$ species. The minor component is probably the polymeric type of species (figure 1(D)).

4.4. Structure during CO oxidation at 623 K

During CO oxidation at 623 K (treatment 4), the structure of the supported V_2O_5 phase does hardly change as compared to that of the air-dehydrated sample (treatment 3). Besides small changes in the Debye–Waller factors, spectra are nearly equal. Furthermore, when oxygen was removed from the feed (treatment 5), no changes in the structure of the XANES and EXAFS spectra are observed. These results indicate that the applied conditions have no impact on the structure of the supported vanadium oxide phase at this temperature.

4.5. Structure during CO oxidation at 723 K

During CO oxidation at 723 K, we have already observed changes in the XANES and EXAFS spectra during the steady-state experiment (treatment 6). This indicates that under the steady-state conditions, the structure of the supported vanadium oxide phase is changed by the reactants. However, when oxygen is removed from the feed at 723 K (treatment 6), more pronounced structural changes occurred. These changes indicate that CO is able to remove oxygen from the catalysts. Reduction brings about removal of oxygen. The XANES data, however, show a change of the local geometry around vanadium from tetrahedral (VO_4) to octahedral (VO_6), i.e., an increased oxygen co-ordination number. This can only be the result of a dramatic structural change of the supported VO_x phase. As was mentioned before, the structure of the reduced vanadium oxide phase has not been resolved yet.

Based on the XANES spectra of the reduced sample, which are represented in figure 12, formation of a distorted octahedral configuration upon reduction is expected. However, the pre-edge position clearly indicates that reduction of the sample by CO had taken place. This means that despite the reduction, an increase of the oxygen co-ordination number has occurred. To our opinion, two explanations could be given for the increase of the oxygen co-ordination number upon reduction of the sample, i.e., formation of bulk V_2O_3 or migration of the V^{3+} ions into the γ-Al_2O_3 lattice.

Haber has suggested that the reduced VO_x phase exists as bulk V_2O_3 on the surface of the support [72]. The structure of V_2O_3 is isomorphous with corundum α-Al_2O_3, in which the oxygen positions are hexagonal close-packed (hcp), with the trivalent cations occupying the octahedral interstices [73]. This results in three vanadium–oxygen bonds of 1.96 Å, and three vanadium–oxygen bonds of 2.06 Å [42,73]. The pre-edge feature in the XANES spectra of the reduced samples makes this structure to be a possible candidate for the analysis of the EXAFS data. However, vanadium neighbours should also be taken into account and we were not able to insert V–V contributions in our fitting procedure. Furthermore, the formation of bulk V_2O_3 upon reduction of the supported vanadium oxide phase could result in the formation of bulk V_2O_5 after re-oxidation of the sample. However, this does not occur and after re-oxidation of the vanadium oxide is redispersed into a monolayer [72]. However, our TPR/TPO experiments did not give an indication of sintering, providing that the oxidised VO_x phase does not re-disperse. On the contrary, the peak maximum of the second TPR has shifted to a higher temperature. Since for V_2O_5 the nucleation-reduction mechanism is operative [74], this is a strong indication that the particles are better dispersed after re-oxidation of the reduced sample.

The other possibility of obtaining a six-fold co-ordination of V^{3+} is migration of the low-valent ions into the γ-Al_2O_3 lattice. Various authors have described processes in which low-valent cations have been incorporated in the

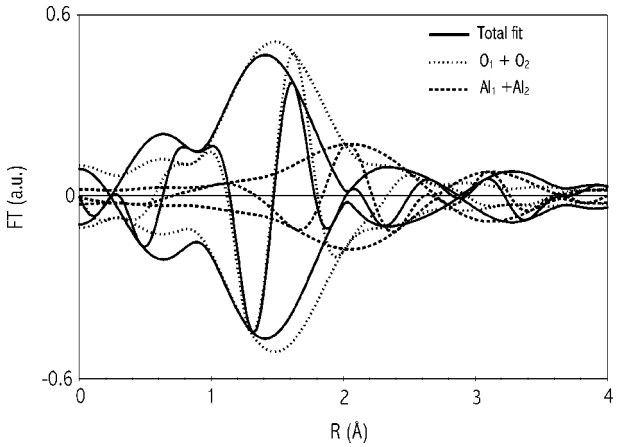

Figure 17. V–O and V–Al contributions and total R-space fit of the reduced sample. Without the V–Al contributions, fit results were not acceptable.

(sub)surface layers of γ-alumina [75–77]. These ions might occupy the tetrahedral and octahedral sites of γ-alumina with the formation of a "surface spinel" [75] or $AlVO_3$ type of compound [78]. We therefore suggest that the V^{3+} ions have migrated into the γ-Al_2O_3 lattice, resulting in the formation of a (surface) ABO_3-type of compound. In literature, only a few examples of such materials are known [78,79]. Reid and Sabine reported the formation of $AlVO_3$ as the result of the H_2 reduction of a physical mixture of V_2O_5 and Al_2O_3 [78]. In this metal-deficient spinel, V^{3+} cations are positioned preferentially in the octahedral Al^{3+} positions of the Al_2O_3 lattice, forcing the Al^{3+} ions into tetrahedral positions [78]. Although in our 17.5 wt% V_2O_5-on-Al_2O_3 catalyst much less vanadium is present, we think that the process is similar. Therefore, we have used the structural parameters of $AlVO_3$ to fit the EXAFS spectrum of the reduced VO_x. The EXAFS data nicely correlate with this model, showing both V–O and V–Al contributions in the spectra. Analysis of the data is complicated, because the V–O and V–Al contributions in the Fourier transforms are strongly interfering and correlated, as can be seen in figure 17. This might explain the absence of V^{3+} EXAFS analysis data in the literature on supported vanadium oxide. However, the data in figure 15 show that the fits for the catalyst after reduction in CO at 723 K are excellent.

We have also performed molecular modelling (force field) on the reduced vanadium oxide-on-alumina system. Preliminary results reveal that V^{3+} ions are not stable on the surface of alumina and that they immediately migrate to an Al^{3+} octahedral position after reduction. However, for most ions (Cr^{3+}, Ni^{2+}), this process is irreversible and re-oxidation of the sample is almost impossible [75,76]. Nevertheless, our TPR/TPO experiments show that it is possible to re-oxidise the reduced vanadium oxide catalyst.

4.6. EXAFS results in relation to the oxidation mechanism

Our XAFS experiments were performed at two different temperatures, i.e., at 623 and 723 K. Based on the results of

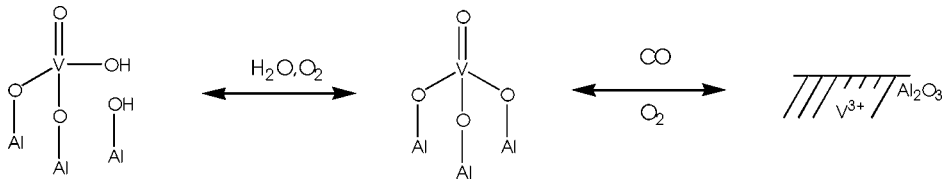

Figure 18. Model for the structure of the supported hydrated, dehydrated and reduced vanadium oxide phase.

Van den Berg, who studied the CO oxidation reaction with V_2O_5-on-Al_2O_3, we expect that the associative mechanism is operative at 623 K [47]. When the associative mechanism is operating, oxidation of CO proceeds via adsorbed oxygen anions, and hence the structure of the supported vanadium oxide phase is not affected by the reactants. No lattice oxygen is consumed and, consequently, the structure of the supported vanadium oxide phase does not change when oxygen was removed from the feed at 623 K (treatment 5). The results of our XAFS experiments at 623 K are in full agreement with the associative mechanism.

When the oxidation reaction obeys the Mars–van Krevelen mechanism, the reaction consumes lattice oxygen. The lattice is subsequently re-oxidised by gas phase oxygen. Our CO oxidation experiments at 723 K show that the catalyst structure was already changing under steady-state conditions, which indicates that lattice oxygen is involved in the oxidation process under these conditions. Furthermore, when oxygen was removed from the feed, the structure of the supported vanadium oxide phase changed completely. This indicates that the reaction proceeds via the Mars–van Krevelen mechanism under these conditions, because structural changes can only appear when lattice oxygen is consumed.

5. Conclusions

In this paper, we have shown that X-ray absorption spectroscopy is a useful tool to monitor the structure of a 17.5 wt% V_2O_5-on-γ-Al_2O_3 catalyst. Experiments were performed *in situ*, i.e., at reaction temperatures and in the presence of reactants. We have used XANES, EXAFS, PCA and TPR/TPO experiments to obtain a better understanding of the structure of the supported vanadium oxide phase and the influence of the reaction conditions on the structure.

The fresh catalyst is hydrated and the vanadium oxide phase consists of a species, which is bound to the support with two oxygen atoms. Furthermore, the vanadium atom is co-ordinated by one vanadyl oxygen atom and one OH group. In agreement with the literature, dehydration to a tetrahedral species occurred during thermal pre-treatment in air. The structure of this $(Al–O)_3–V{=}O$ remained stable under steady-state CO oxidation conditions at 623 and 723 K. However, when oxygen was removed from the feed at 723 K the X-ray absorption spectra dramatically changed. These changes were the result of reduction of the vanadium species. EXAFS data analysis of the reduced species was complicated, but showed that the reduced vanadium ions migrate into the surface layers of -Al_2O_3. Figure 18 represents a model for our findings. This process was confirmed by molecular modelling. We think that this process is reversible, and that the $(Al–O)_3–V{=}O$ species are restored after re-oxidation. To our knowledge, this is the first time that the structure of the V^{3+} phase is confirmed by experimental data.

Our results show that the structure of a well-dispersed supported oxide phase is very sensitive for the applied conditions (temperature, type of reactants). Therefore, X-ray absorption spectroscopy is a powerful tool to study these changes in relation with the reaction mechanism *in situ*, i.e., at reaction temperatures and in the presence of reactants. Although we realise that X-ray absorption spectroscopy cannot be used as a stand-alone mechanistic characterisation technique, the application of XANES and EXAFS to investigate the mechanism of oxidation reactions is an additional tool and catalytic experiments and $^{18}O/^{16}O$ scrambling experiments will be necessary to complete the picture.

References

[1] X. Gao, S.R. Bare, B.M. Weckhuysen and I.E. Wachs, J. Phys. Chem. B 102 (1998) 10842.
[2] I.E. Wachs, Catal. Today 27 (1996) 437.
[3] G.T. Went and S.T. Oyama, J. Phys. Chem. 94 (1990) 4240.
[4] F. Roozeboom, M.C. Mittelmeijer-Hazeleger, J.A. Moulijn, J. Medema, V.H.J. de Beer and P.J. Gellings, J. Phys. Chem. 84 (1980) 2783.
[5] G. Busca, Mater. Chem. Phys. 19 (1988) 157.
[6] A.A. Davydov, Kinet. Katal. 34 (1993) 951.
[7] T. Tanaka, H. Yamashita, R. Tsuchitani, T. Funabiki and S. Yoshida, J. Chem. Soc. Faraday Trans. I 84 (1988) 2987.
[8] S. Yoshida, T. Tanaka, Y. Nishimura, H. Mizutani and T. Funabiki, *Proc. ICC IX* (1988) p. 1473.
[9] S. Yoshida, T. Tanaka, T. Hanada, T. Hiraiwa and H. Kanai, Catal. Lett. 12 (1992) 277.
[10] R. Kozlowski, R.F. Pettifer and J.M. Thomas, J. Phys Chem. 87 (1983) 5176.
[11] J. Haber, A. Kozlowska and R. Kozlowski, J. Catal. 102 (1986) 52.
[12] N. Das, H. Eckert, H. Hu, I.E. Wachs, J.F. Walzer and F.J. Feher, J. Phys. Chem. 97 (1993) 8240.
[13] H. Eckert and I.E. Wachs, Mater. Res. Soc. Symp. Proc. 111 (1988) 455.
[14] H. Eckert and I.E. Wachs, J. Phys. Chem. 93 (1989) 6796.
[15] L.R. Le Costumer, B. Taouk, M. Le Meur, E. Payen, M. Guelton and J.M. Grimblot, J. Phys. Chem. 92 (1988) 1230.
[16] B.M. Weckhuysen, I.P. Vannijvel and R.A. Schoonheydt, Zeolites 15 (1995) 482.
[17] U. Scharf, M. Schraml-Merth, A. Wokaun and A. Baiker, J. Chem. Soc. Faraday Trans. 87 (1991) 3299.
[18] G. Catana, R. Ramachandra Rao, B.M. Weckhuysen, P. van der Voort, E. Vansant and R. Schoonheydt, J. Phys. Chem. B 102 (1998) 8005.

[19] M.F. Hazenkamp and G. Blasse, J. Phys. Chem. 96 (1992) 3442.
[20] M. Anpo, M. Sunamoto and M. Che, J. Phys. Chem. 93 (1989) 1187.
[21] G. Busca and E. Giamello, Mater. Chem. Phys. 25 (1990) 475.
[22] B.I. Wittington and J.R. Anderson, J. Phys. Chem. 97 (1993) 1032.
[23] J.M. Jehng, G. Deo, B.M. Weckhuysen and I.E. Wachs, J. Mol. Catal. A 110 (1996) 41.
[24] I.E. Wachs and B.M. Weckhuysen, Appl. Catal. A 157 (1997) 67.
[25] S.S. Chan, I.E. Wachs, L.L. Murrell, L. Wang and W.K. Hall, J. Phys. Chem. 88 (1984) 5831.
[26] X. Gao, S.R. Bare, B.M. Weckhuysen and I.E. Wachs, J. Phys. Chem. B 102 (1998) 10684.
[27] T. Kataoka and J.A. Dumesic, J. Catal. 112 (1988) 66.
[28] G.C. Bond, J. Perez Zurita, S. Flamerz, P.J. Gellings, H. Bosch, J.G. van Ommen and B.J. Kip, Appl. Catal. 22 (1986) 361.
[29] W. Fluhr, M. Schraml-Marth, A. Wokaun and A. Baiker, Ber. Bunsenges Phys. Chem. 8 (1989) 852.
[30] I.E. Wachs, G. Deo, B.M. Weckhuysen, V.V. Guliants and J.B. Benziger, Catal. Today 32 (1996) 47.
[31] G. Ramis, C. Cristiani, P. Forzatti and G. Busca, J. Catal. 124 (1990) 574.
[32] I.E. Wachs, R.Y. Saleh, S.S. Chan and C.C. Chersich, Appl. Catal. 15 (1985) 339.
[33] K. Mori, M. Inomata, A. Miyamoto and Y. Murakami, J. Chem. Soc. Faraday Trans. I 80 (1984) 2666.
[34] T. Tanaka, Y. Nishimura, S. Kawasaki, M. Oe, T. Funabiki and S. Yoshida, J. Catal. 118 (1989) 327.
[35] S.L. Kaliaguine, B.N. Shelimov and B. Kazansky, J. Catal. 55 (1978) 384.
[36] A.A. Siddiqi and J.W. Tenini, Hydrocarbon Process. 60 (1984) 649.
[37] M. Iwamoto, J. Hirata, K. Matsukami and S. Kagawa, J. Phys. Chem. 87 (1983) 903.
[38] G.I. Golodets, Stud. Surf. Sci. Catal. 55 (1990) 693.
[39] P. Mars and D.W. van Krevelen, Chem. Eng. Sci. (Special Suppl.) 3 (1954) 41.
[40] A.J. Van Dillen, Catalytic oxidation of carbon monoxide over oxides of indium and vanadium, Thesis, Utrecht University (1977).
[41] L.V. Azararoff and D.M. Pease, in: *X-Ray Spectroscopy*, ed. L.V. Azaroff (McGraw Hil, New York, 1974).
[42] J. Wong, F.W. Lytle, R.P. Mesmer and D.H. Maylotte, Phys. Rev. B 30 (1984) 5596.
[43] J. Wong, R.P. Mesmer, D.H. Maylotte and F.W. Lytle, in: *EXAFS and Near Edge Structure*, eds. A. Bianconi, L. Inoccia and S. Stipcich (Springer, Berlin, 1983) p. 130.
[44] J. Wong, D.H. Maylotte, F.W. Lytle, R.B. Greegor and R.L.St. Peters, in: *EXAFS and Near Edge Structure*, eds. A. Bianconi, L. Inoccia and S. Stipcich (Springer, Berlin, 1983) p. 206.
[45] I. Davoli, S. Stizza, M. Benfatto, O. Gzowski, L. Murawski and A. Bianconi, in: *EXAFS and Near Edge Structure*, eds. A. Bianconi, L. Inoccia and S. Stipcich (Springer, Berlin, 1983) p. 162.
[46] M. Ruitenbeek, R.A. Overbeek, A.J. van Dillen, D.C. Koningsberger and J.W. Geus, Recl. Trav. Chim. Pays-Bas 115 (1996) 519.
[47] J. van den Berg, Stoichiometry and catalytic activity of vanadia-based oxides for the oxidation of CO and H_2, Thesis, Utrecht University (1984).
[48] I.E. Wachs, J.-M. Jehng, G. Deo, B.M. Weckhuysen, V.V. Guliants, J.B. Benziger and S. Sundaresan, J. Catal. 170 (1997) 75.
[49] F.W.H. Kampers, T.M.J. Maas, J. van Grondelle, P. Brinkgreve and D.C. Koningsberger, Rev. Sci. Instrum. 60 (1989) 2635.
[50] M. Vaarkamp, B.L. Mojet, F.S. Modica, J.T. Miler and D.C. Koningsberger, J. Phys. Chem. 99 (1995) 16067.
[51] http://www.xs4all.nl/∼xsi/.
[52] M. Vaarkamp, I. Dring, R.J. Oldman, E.A. Stern and D.C. Koningsberger, Phys. Rev. B 50 (1994) 7872.
[53] J.W. Cook, Jr. and D.E. Sayers, J. Appl. Phys. 52 (1981) 5024.
[54] J.B.A.D. van Zon, D.C. Koningsberger, H.F.J. van 't Blik and D.E. Sayers, J. Chem. Phys. 82 (1985) 5742.
[55] E. Vogt, Preparation and properties of catalysts supported on modified silica, Thesis, Utrecht University (1988).
[56] B.L. Mojet, Metal support interactions, a step closer to the origin, Thesis, Utrecht University (1997).
[57] F.W.H. Kampers, EXAFS in catalysis, instrumentation and applications, Thesis, TU Eindhoven (1988).
[58] J.N. Fiedor, A. Proctor, M. Houalla and D.M. Hercules, Surf. Interface Anal. 20 (1993) 1.
[59] S.J. Scierka, A. Proctor, J.N. Fiedor and D.M. Hercules, Surf. Interface Anal. 20 (1993) 901.
[60] M.A. Eberhardt, A. Proctor, M. Houalla and D.M. Hercules, J. Catal. 160 (1996) 27.
[61] M.J. Fay, A. Proctor, D.P. Hoffmann, M. Houalla and D.M. Hercules, Mikrochim. Acta 109 (1992) 281.
[62] E.R. Malinowski, *Factor Analysis in Chemistry*, 2nd Ed. (Wiley, New York, 1991).
[63] E.R. Malinowski, J. Chemom. 3 (1988) 49.
[64] E.R. Malinowski, J. Chemom. 4 (1990) 102.
[65] F.M. Dautzenberg, ACS Symposium Series 421 (1989) 277.
[66] M. Ruitenbeek, Characterisation of vanadium-based oxidation catalysts, Thesis, Utrecht University (1999).
[67] D.E. Ramaker, B.L. Mojet, D.C. Koningsberger and W.E. O'Grady, J. Phys. Condens. Matter 10 (1998) 8753.
[68] F.M.F. de Groot, M. Ruitenbeek and D.C. Koningsberger, to be published.
[69] H. Praliaud and M.-V. Mathieu, J. Chim. Phys. 73 (1976) 689.
[70] F. Lemoigno, E. Prouzet, Z.Y. Wu, P. Gressier and G. Ouvrard, J. Phys. IV France 7 (1997) 263.
[71] W.A. Caliebe, C.-C. Kao, J.B. Hastings, M. Taguchi, A. Kotani, T. Uozumi and F.M.F. de Groot, Phys. Rev. B 58 (1998) 13452.
[72] J. Haber, in: *Catalytic Oxidation, Principles and Applications*, eds. R.A. Sheldon and R.A. van Santen (World Scientific, London, 1995) p. 17.
[73] R.E. Newnham and Y.M. de Haan, Z. Kristall. 117 (1962) 235.
[74] N.W. Hurst, S.J. Gentry, A. Jones and B.D. McNicol, Catal. Rev. Sci. Eng. 24 (1982) 233.
[75] W.S. Xia, H.L. Wan and Y. Chen, J. Mol. Catal. A 138 (1999) 185.
[76] B.M. Weckhuysen, L.M. de Ridder, P.J. Grobet and R.A. Schoonheydt, J. Phys. Chem. 99 (1995) 320.
[77] B.M. Weckhuysen and R.A. Schoonheydt, Catal. Today 51 (1999) 223.
[78] A.F. Reid and T.M. Sabine, J. Solid State Chem. 2 (1970) 203.
[79] B. Reuter, R. Aust, G. Collsmann and Ch. Neuwald, Z. Anorg. Allg. Chem. 500 (1983) 188.